

The Ruderman-Kittel-Kasuya-Yosida (RKKY) interaction across a tunneling junction out of equilibrium

N. F. Schwabe and R. J. Elliott

University of Oxford, Department of Physics,

Theoretical Physics, 1 Keble Road, Oxford OX1 3NP, United Kingdom

Ned S. Wingreen

NEC Research Institute, 4 Independence Way, Princeton NJ 08540, USA

(May 6, 2021)

Abstract

The Ruderman-Kittel-Kasuya-Yosida (RKKY) interaction between two magnetic s - d spin impurities across a tunneling junction is studied when the system is driven out of equilibrium through biasing the junction. The nonequilibrium situation is handled with the Keldysh time-loop perturbation formalism in conjunction with appropriate coupling methods for tunneling systems due to Caroli and Feuchtwang. We find that the presence of a nonequilibrium bias across the junction leads to an interference of several fundamental oscillations, such that in this tunneling geometry, it is possible to tune the interaction between ferromagnetic and antiferromagnetic coupling at a fixed impurity configuration, simply by changing the bias across the junction. Furthermore, it is shown that the range of the RKKY interaction is altered out of equilibrium, such that in particular the interaction energy between two slabs of spins scales extensively with the thickness of the slabs in the presence of an applied bias.

PACS numbers: 75.30Et, 73.40Gk, 85.30Mn, 75.70-i

Typeset using REVTeX

I. INTRODUCTION

The Ruderman-Kittel-Kasuya-Yosida (RKKY) interaction has been a very intensely studied phenomenon in solid state physics since it was first proposed as an interaction between nuclear spins^{1,2}, and later between localized electronic spins in metals³. More recently studies of the interaction have focussed on its effects in various structured systems and in particular on the role it plays in the giant magnetoresistance effects observed in some layered structures of magnetic and non-magnetic materials⁴⁻⁷.

Furthermore it has been suggested that the RKKY interaction is responsible for spin polarization effects observed in tunneling systems⁸, such as layered structures with a potential barrier formed by an insulating oxide layer or a vacuum gap. For arrangements involving movable (vacuum) tunneling junctions, such as those occurring in scanning tunneling microscopy (STM) it has been suggested that the exchange interaction between two magnetic materials on either side of the tunneling junction can be used in a modified version of atomic force microscopy, which may be called exchange force microscopy, in order to resolve an atomic image of a sample structure^{9,10}.

Particularly in tunneling systems, the measurement of electronic properties, such as for example the electronic density of states, intrinsically requires the structure to be biased out of equilibrium. The presence of a nonequilibrium bias may also occur in structures which exhibit giant magnetoresistance phenomena, when parts of the structure contain a potential barrier. To date, however, descriptions of the RKKY interaction are confined to systems in equilibrium, including approximate theoretical treatments of the interaction across a potential well⁴ and a tunneling barrier¹⁰.

It is therefore the purpose of the present paper to establish a theoretical description of the RKKY-interaction across a tunneling barrier out of equilibrium from first principles. For this purpose we employ the Keldysh nonequilibrium perturbation formalism¹¹ along with a coupling procedure for structured systems developed by Caroli, Combescot *et al.*¹²⁻¹⁵ and Feuchtwang¹⁶⁻¹⁸, leading to a proper nonequilibrium field theoretic description. Since the

treatments by Caroli and Feuchtwang are proper many-body formalisms their application to the present problem simultaneously provides the basis for the inclusion of further many-body effects such as carrier-carrier or carrier-phonon interactions to the problem.

With this technique we manage to derive a general nonequilibrium solution for the RKKY interaction for various dimensionalities and arrangements of spins within a structured system. Particularly we show that the interaction of spins across a tunneling junction can be tuned between ferromagnetic (FM) and antiferromagnetic (AFM) coupling by changing the bias across the junction alone. For the application to exchange force microscopy, mentioned before, it is shown that varying the bias across the vacuum junction in an STM can lead to a force which switches between attractive and repulsive behavior and that this force should be experimentally measurable with a state of the art apparatus. Furthermore, we show that the presence of a nonequilibrium bias across the junction significantly alters the range of the RKKY interaction, such that in particular the interaction energy between two slabs of spins scales extensively with the thickness of the slabs.

The remainder of the paper is structured as follows: In Sec. II we establish a model of the tunneling system containing the spin impurities. Sec. III contains a derivation of the RKKY interaction out of equilibrium in various dimensions in terms of general Keldysh nonequilibrium Green's functions. In Sec. III A we consider the interaction of two magnetic *s-d* impurities across a one dimensional tunneling junction out of equilibrium and in Sec. III B we extend these results to the more realistic situation of two magnetic layers or slabs of spins on either side of a planar three dimensional tunneling junction, including the possibility of a non-magnetic spacer material between the magnetic materials and the barrier. Sec. IV describes how the Keldysh Green's functions used in Sec. III are obtained in a system containing a potential barrier. In Sec. V we implement our results numerically and calculate equilibrium and nonequilibrium versions of the RKKY interaction for various tunneling geometries. Sec. VI discusses the experimental observability of the behavior of the interaction predicted by the numerical study. In Sec. VII, in conclusion, the implications and possible further applications of this work are summarized.

II. THE MODEL

The one dimensional tunneling system we consider consists of a tunneling barrier which is connected to two leads on the left and right at the points L and R , respectively, as shown in Fig. 1. In equilibrium the barrier is assumed to be flat on top with an abrupt potential change of V_0 at the interfaces. The corresponding single particle potential can be written as

$$V(x) = V_0 \Theta(x - L) \Theta(R - x). \quad (1)$$

Upon biasing the junction, the potential of the barrier acquires a slope and the chemical potential μ^R in the right lead undergoes a shift eV with respect to the chemical potential μ^L in the left lead. Simultaneously, the conduction band bottom V^R in the right lead shifts by eV with respect to conduction band bottom V^L in the left lead, such that the electronic potential is changed to

$$V(x) = \left[V_0 - eV \frac{x - L}{R - L} \right] \Theta(x - L) \Theta(R - x) - eV \Theta(x - R). \quad (2)$$

Here the bottom of the conduction band on the left side is taken as the origin of energy, e is the modulus of the elementary charge of an electron, and V the voltage drop across the barrier.

Two magnetic s - d impurities are situated within the electrodes, on either side of the barrier, at an equal distance d from the interfaces. For simplicity, both electrodes are considered to consist of the same material and the effective electron masses are assumed to be equal in all three parts of the junction.

The Hamiltonian of the system, with a single electron band in each part of the junction, can be written as

$$H = \sum_{\alpha} \int dx \Psi_{\alpha}^{\dagger}(x) \left[\frac{p^2}{2m} + V(x) \right] \Psi_{\alpha}(x) - \frac{J}{2} \sum_{p=1,2;\alpha,\beta} \boldsymbol{\sigma}_{\alpha\beta} \cdot \mathbf{S}_p \int dx \Psi_{\alpha}^{\dagger}(x) \delta(x - x_p) \Psi_{\beta}(x) = H_0 + H_{s-d}, \quad (3)$$

where H_{s-d} is the last, spin dependent, term in the Hamiltonian and the coupling constant J is assumed to have the units Jm^d , where d is the dimensionality of the system considered.

Here a space representation has been chosen, which proves to be advantageous due to the lack of translational invariance caused by the presence of the barrier potential $V(x)$. $p^2/2m$ is the kinetic energy of electrons with uniform effective mass m , and we use $\hbar \equiv 1$ throughout. $\boldsymbol{\sigma}_{\alpha\beta}$ is the vector of Pauli matrices, used to represent the spin of the conduction electrons which couple to the two local moments \mathbf{S}_p . The indices α and β label the two spin components: $\alpha, \beta \in \{\uparrow, \downarrow\}$.

III. EXPRESSION FOR THE RKKY INTERACTION

A. The interaction in one dimension

The RKKY interaction energy between the two impurities is calculated from the lowest order exchange contributions to the perturbation of the energy of the localized spins in the presence of the conduction electrons. Either in or out of equilibrium this energy is given by the expectation value $\langle H_{s-d} \rangle_{(1\text{ex})}$, where the subscript (1ex) indicates that only the first order exchange contributions to the average are considered. Effectively, therefore, one has to calculate the first order perturbation to the conduction electron spin density due to the first spin at the location of the second spin and *vice versa*^{1,19}. The total interaction energy is a sum of these two contributions

$$E_{\text{RK}} = -\frac{J}{2} \sum_{p=1,2} \mathbf{S}_p \cdot \Delta \boldsymbol{\rho}_{(1\text{ex})}(x_p), \quad (4)$$

where

$$\Delta \boldsymbol{\rho}_{(1\text{ex})}(x_p) = \sum_{\alpha,\beta} \boldsymbol{\sigma}_{\alpha\beta} \langle n_{\alpha\beta}(x_p) \rangle_{(1\text{ex})} = \sum_{\alpha,\beta} \boldsymbol{\sigma}_{\alpha\beta} \langle \Psi_{\alpha}^{\dagger}(x_p) \Psi_{\beta}(x_p) \rangle_{(1\text{ex})} \quad (p \in \{1, 2\}) \quad (5)$$

is the first order exchange contribution to the spin density at site p .

In the present case we now have to calculate (4) by means of (5) out of equilibrium. In order to do so we make use of the Keldysh formalism. In the Keldysh notation the spin dependent particle density correlation function $\langle n_{\alpha\beta}(x) \rangle = \langle \Psi_{\alpha}^{\dagger}(x) \Psi_{\beta}(x) \rangle$ can be written in terms of the Keldysh Green's function $G_{\alpha\beta}^{<}(x, t; x', 0)$ which is defined as

$$G_{\alpha\beta}^<(x, t; x', 0) = i\langle \Psi_{\beta}^{\dagger}(x', 0) \Psi_{\alpha}(x, t) \rangle, \quad (6)$$

where the operators $\Psi_{\alpha}^{\dagger}(x, t)$ and $\Psi_{\alpha}(x, t)$ are the field operators of the system considered, which create and destroy a particle with spin α at point x and time t , respectively. From this we find

$$\langle n_{\alpha\beta}(x) \rangle = -i \lim_{\substack{t \rightarrow 0 \\ x' \rightarrow x}} \int_{-\infty}^{\infty} \frac{d\omega}{2\pi} e^{i\omega t} G_{\alpha\beta}^<(x, x'; \omega). \quad (7)$$

Using the definition of $G^<$, it can be shown in equilibrium that this expression is equivalent to the usual relation between the particle density and the retarded Green's function G^r ,

$$\langle n_{\alpha\beta}(x) \rangle = -\frac{1}{\pi} \lim_{x' \rightarrow x} \int_{-\infty}^{\infty} n_F(\omega) \text{Im} [G_{\alpha\beta}^r(x, x'; \omega)] d\omega, \quad (8)$$

where $n_F(\omega) = \{\exp[\beta(\omega - \mu)] + 1\}^{-1}$ is the usual Fermi distribution function in equilibrium, μ is the equilibrium chemical potential and G^r is the retarded Green's function of the system, which is defined as

$$G_{\alpha\beta}^r(x, x'; t) = -i\Theta(t) \langle \{ \Psi_{\beta}^{\dagger}(x', 0), \Psi_{\alpha}(x, t) \} \rangle, \quad (9)$$

where $\{ , \}$ denotes the anti-commutator. The advanced Green's function G^a

$$G_{\alpha\beta}^a(x, x'; t) = i\Theta(-t) \langle \{ \Psi_{\beta}^{\dagger}(x', 0), \Psi_{\alpha}(x, t) \} \rangle, \quad (10)$$

will be used later.

In order to obtain a proper nonequilibrium result for the RKKY interaction we have to perform first order nonequilibrium perturbation theory on expression (7). The appropriate formalism, introduced by Keldysh, reformulates the regular diagrammatic perturbation theory in terms of a 2×2 matrix formalism, to properly handle the time development, since out of equilibrium the usual S -matrix expansion based on the Gell-Mann-Low theorem breaks down^{11,20}. The Green's function matrix of the unperturbed system without spin impurities, but including the full barrier potential within this formalism is written as

$$\mathbf{G}_{(0)\alpha\beta}(x, x'; t) = \begin{pmatrix} G_{(0)\alpha\beta}^t(x, x'; t) & -G_{(0)\alpha\beta}^<(x, x'; t) \\ G_{(0)\alpha\beta}^>(x, x'; t) & -G_{(0)\alpha\beta}^{\bar{t}}(x, x'; t) \end{pmatrix}. \quad (11)$$

G^t and $G^{\tilde{t}}$ denote the usual time-ordered and anti-time-ordered Green's functions with the general definitions

$$G_{\alpha\beta}^t(x, x'; t) = -i\langle T\Psi_\alpha(x, t)\Psi_\beta^\dagger(x', 0)\rangle, \quad (12)$$

$$G_{\alpha\beta}^{\tilde{t}}(x, x'; t) = -i\langle \tilde{T}\Psi_\alpha(x, t)\Psi_\beta^\dagger(x', 0)\rangle, \quad (13)$$

where T and \tilde{T} are the time-ordering and anti-time-ordering operators, respectively. $G^>$ is the complementary correlation function to $G^<$:

$$G_{\alpha\beta}^>(x, x'; t) = -i\langle \Psi_\alpha(x, t)\Psi_\beta^\dagger(x', 0)\rangle. \quad (14)$$

The corresponding matrix perturbation expansion to first order in the coupling J yields

$$\begin{aligned} \mathbf{G}_{(1)\alpha\beta}(x_p, x_p; t - t') &= \mathbf{G}_{(0)\alpha\beta}(x_p, x_p; t - t')\delta_{\alpha,\beta} \\ &- \frac{J}{2} \sum_{q=1,2} \mathbf{S}_q \cdot \boldsymbol{\sigma}_{\beta\alpha} \int dt_1 \mathbf{G}_{(0)\alpha\alpha}(x_p, x_q; t - t_1) \mathbf{G}_{(0)\beta\beta}(x_q, x_p; t_1 - t'). \end{aligned} \quad (15)$$

From (15) the first order exchange terms of the function $G^<$ can be resolved as

$$\begin{aligned} G_{(1\text{ex})\alpha\beta}^<(x_p, x_p; t - t') &= -\frac{J}{2} \mathbf{S}_q \cdot \boldsymbol{\sigma}_{\beta\alpha} \int dt_1 \left[G_{(0)}^<(x_p, x_q; t - t_1) G_{(0)}^a(x_p, x_q; t_1 - t') \right. \\ &+ \left. G_{(0)}^r(x_p, x_q; t - t_1) G_{(0)}^>(x_p, x_q; t_1 - t') \right] \quad (p \in \{1, 2\}, q \neq p), \end{aligned} \quad (16)$$

where we have now dropped the spin indices in the unperturbed Green's functions since they are spin independent. To obtain (16), we have used appropriate relations between the six Green's functions $G^<$, $G^>$, G^t , $G^{\tilde{t}}$, G^r and G^a in order to replace the dependence of the result on G^t and $G^{\tilde{t}}$ by one on G^r and G^a (cf. Ref. 20).

One relation arising from this transformation that holds generally for operators in the Keldysh formalism and which is particularly useful to us is

$$(AB)^< = A^< B^a + A^r B^<, \quad (17)$$

where AB is to be understood as a matrix product of two general operators A and B , implying integrations over space and time where applicable. By means of Fourier transformation of (16) into the frequency domain, (4) can therefore be expressed as

$$\begin{aligned}
E_{\text{RK}} = & J^2 \mathbf{S}_1 \cdot \mathbf{S}_2 \int_{-\infty}^{\infty} \text{Im} \left[G_{(0)}^<(x_1, x_2) \right. \\
& \times \left. \{ G_{(0)}^r(x_2, x_1) + G_{(0)}^a(x_2, x_1) \} \right] \frac{d\omega}{2\pi}.
\end{aligned} \tag{18}$$

The above equation is the general expression for the RKKY interaction out of equilibrium in a purely 1D system without translational invariance. It is one of the central results of the present work and the principal goal of the following treatment is to evaluate it explicitly for various situations.

In an equilibrium situation it is easily established that (18) goes over to the well known result^{21,22}

$$\begin{aligned}
E_{\text{RK}} = & -\frac{1}{\pi} J^2 \mathbf{S}_1 \cdot \mathbf{S}_2 \int_{-\infty}^{\infty} n_F(\omega) \\
& \times \text{Im} \left[G_{(0)}^r(x_1, x_2) G_{(0)}^r(x_2, x_1) \right] d\omega.
\end{aligned} \tag{19}$$

Before we establish how the Keldysh Green's functions $G_{(0)}^<$ and $G_{(0)}^{r/a}$ are calculated in a nonequilibrium situation we will generalize the results just obtained to higher dimensions.

B. Generalization to two and three dimensions

For the extension to higher dimensions we assume that the system is translationally invariant in the further one or two dimensions, corresponding to a perfectly planar barrier. Once we have found the solution for the purely 1D Green's function $G_{(0)}^{1\text{D}}$, we can simplify the solution of the planar extension of the equivalent problem by exploiting the translational invariance of the system in the additional directions parallel to the barrier by means of corresponding Fourier transforms

$$G_{(0)}^{2/3\text{D}}(x, x'; \mathbf{k}_{\parallel}; \omega) = \int d^{d-1} \mathbf{r} e^{i\mathbf{k}_{\parallel} \cdot \mathbf{r}} G_{(0)}^{2/3\text{D}}(\mathbf{x}, \mathbf{x}'; \omega), \tag{20}$$

where \mathbf{x} is a d -dimensional coordinate, $\mathbf{r} = \mathbf{x}_{\parallel} - \mathbf{x}'_{\parallel}$ is the $(d-1)$ -dimensional relative position vector parallel to the barrier and \mathbf{k}_{\parallel} denotes the $(d-1)$ -dimensional electron wavevector parallel to the barrier, where $d \in \{2, 3\}$. In the following we shall drop the superscripts again

that were just introduced to indicate the dimensionality of the system which the corresponding Green's functions describe, since it will be always recognizable from the arguments of these functions whether they pertain to a purely 1D system or to a planar version in higher dimensions.

The extension to 2/3D leaves the spatial dependence of the Hamiltonian unaffected in the direction perpendicular to the barrier and, as will be shown in Sec. IV, only amounts to a change in the energy arguments of the corresponding Green's functions (see also Ref. 18). The expression for the RKKY interaction between two arbitrarily placed impurities with respect to the barrier in d -dimensions can then be written as an extension from (18)

$$\begin{aligned}
E_{\text{RK}} = & J^2 \mathbf{S}_1 \cdot \mathbf{S}_2 \int \frac{d^{d-1} \mathbf{q}_{\parallel} d^{d-1} \mathbf{k}_{\parallel}}{(2\pi)^{(2d-2)}} e^{-i \mathbf{q}_{\parallel} \cdot \mathbf{r}_{12}} \\
& \times \int_{-\infty}^{\infty} \text{Im} \left[G_{(0)}^<(x_1, x_2; \mathbf{q}_{\parallel} - \mathbf{k}_{\parallel}; \omega) \right. \\
& \times \left. \{ G_{(0)}^r(x_2, x_1; \mathbf{k}_{\parallel}; \omega) + G_{(0)}^a(x_2, x_1; \mathbf{k}_{\parallel}; \omega) \} \right] \frac{d\omega}{2\pi} \\
& (d \in \{2, 3\}),
\end{aligned} \tag{21}$$

where \mathbf{r}_{12} denotes the impurity displacement in the direction parallel to the barrier.

The most immediate application of the present theory is in a 3D tunneling system where the interaction between either two monolayers or two slabs of spins across a barrier is of interest for the description of giant magnetoresistance phenomena⁴⁻⁷. It will be assumed that all spins within one monolayer or slab have the same orientation due to a predominant ferromagnetic coupling over short distances. In equilibrium and without a barrier it was pointed out by Yafet²³ how the interaction between two monolayers can be obtained from the conventional 3D version. In our case the corresponding expression is obtained through integrating over all \mathbf{r}_{12} and subsequently over \mathbf{q}_{\parallel} in (21):

$$\begin{aligned}
E_{\text{RK}}^{\text{m}} = & \left(J \rho_{s-d}^{2D} \right)^2 \nu^{2D} \mathbf{S}_1 \cdot \mathbf{S}_2 \int \frac{d^2 \mathbf{k}_{\parallel}}{(2\pi)^2} \int_{-\infty}^{\infty} \text{Im} \left[G_{(0)}^<(x_1, x_2; -\mathbf{k}_{\parallel}; \omega) \right. \\
& \times \left. \{ G_{(0)}^r(x_2, x_1; \mathbf{k}_{\parallel}; \omega) + G_{(0)}^a(x_2, x_1; \mathbf{k}_{\parallel}; \omega) \} \right] \frac{d\omega}{2\pi},
\end{aligned} \tag{22}$$

where E_{RK}^{m} is now the monolayer interaction energy across the junction, ν^{2D} is the surface

area of the junction and ρ_{s-d}^{2D} is the surface density of the s - d spins in each of the two planes parallel to the barrier.

The situation where two finite slabs of spins interact across a finite spacer layer which contains the barrier is shown schematically in Fig. 2. The interaction between two slabs of spins across a planar tunneling barrier can be obtained by summing the contributions coming from each pair of interacting monolayers involved. In the present case where a continuous system is considered this amounts to two spatial integrations of the monolayer interaction in (22) in the direction perpendicular to the barrier. If, for simplicity, we consider two interacting slabs of the same thickness l which are symmetrically displaced from the barrier, these two integrations assume the form

$$E_{\text{RK}}^s = \left(\rho_{s-d}^{3D}\right)^2 \int_{L-(d+l)}^{L-d} dx_1 \int_{R+d}^{R+(d+l)} dx_2 \left[\frac{E_{\text{RK}}^m(x_1, x_2)}{\left(\rho_{s-d}^{2D}\right)^2} \right], \quad (23)$$

where E_{RK}^s is the interaction energy of the two slabs and in $E_{\text{RK}}^m(x_1, x_2)$, is taken from (22) where x_1 indicates a position within the left electrode and x_2 one within the right one, respectively, and ρ_{s-d}^{3D} is the 3D density of s - d spins within the slabs.

Now that formal expressions for the RKKY interaction are in hand, the next step is the evaluation of the Keldysh Green's functions $G_{(0)}^<(x, x')$ and $G_{(0)}^{r/a}(x, x')$ of the nonequilibrium 1D system and their extensions to higher dimensions.

IV. EVALUATION OF THE RELEVANT GREEN'S FUNCTIONS

It has been established by Caroli¹²⁻¹⁵ and Feuchtwang¹⁶⁻¹⁸, that a tunneling system out of equilibrium can be treated by partitioning the system into several uncoupled parts which are considered to be in equilibrium at $t = -\infty$. These parts are subsequently coupled to each other through appropriate transfer terms, in conjunction with an adiabatic switching procedure, to finally yield a nonequilibrium steady state. Formally, this corresponds to a perturbation expansion of these transfer terms to all orders^{12,13}, but it can also be shown to be equivalent to applying Green's theorem at the partitioning points^{16,17}. The number of

partitions to be made in the system is in principle arbitrary and will largely depend on the geometry considered. In the present case with a possibly sloping tunneling barrier of finite width, a partitioning into three regions at the electrode-barrier interfaces L and R – shown by the vertical dashed lines in Fig. 1 – is most convenient. In the present treatment we will follow closely the approach of Ref. 17 for continuous systems. The Hamiltonian H_0 in (3) is consequently written as a sum of three independent parts

$$\begin{aligned} H_0(x) = & \Theta(L - x)H_L(x) \\ & + \Theta(x - L)\Theta(R - x)H_B(x) + \Theta(x - R)H_R(x). \end{aligned} \quad (24)$$

A. Green's functions in one dimension

In one dimension the Green's function $G_{(0)}$ of the system including the barrier has to satisfy the inhomogeneous Schrödinger equation

$$[\omega - H_0(x)]G_{(0)}(x, x'; \omega) = \delta(x - x'). \quad (25)$$

Similarly one can define Green's functions for the several uncoupled sub-parts of the system $\eta \in \{L, B, R\}$ as

$$[\omega - H_\eta(x)]g_\eta(x, x'; \omega) = \delta(x - x'), \quad (26)$$

where x, x' lie within the appropriate region determined by the choice of η . Additionally, these functions have to satisfy appropriate boundary conditions at the electrode-barrier interfaces R and L . In principle these boundary conditions can be an arbitrary mixture of the Dirichlet and Neumann type. However, for simplicity it is best to use one or the other exclusively, and we choose here the Dirichlet conditions that the Green's functions vanish if they are taken with one of their arguments on the respective interfaces R or L . Relations between these uncoupled Green's functions g_η and the Green's function $G_{(0)}$ of the full system, satisfying (25), can be established, as noted before, by means of Green's theorem

applied at the interfaces. If in addition the discontinuity conditions for the derivatives of the full Green's function $G_{(0)}$ are used

$$\partial_x G_{(0)}(x, x') \Big|_{x=x'^-}^{x=x'^+} = 2m = \partial_{x'} G_{(0)}(x, x') \Big|_{x'=x^-}^{x'=x^+}, \quad (27)$$

(where we have left out the energy argument for brevity), together with appropriately chosen versions of further continuity conditions

$$G_{(0)}(x, x') \Big|_{x=x'^-}^{x=x'^+} = 0, \quad (28)$$

$$\partial_x \partial_{x'} G_{(0)}(x, x') \Big|_{x=x'^-}^{x=x'^+} = 0, \quad (29)$$

which this function has to satisfy, one can find $G_{(0)}(x, x')$. In the simple cases where $x, x' \in \{L, R\}$, the full Green's function can be written as¹⁷

$$\begin{aligned} & \begin{pmatrix} G_{(0)}(L, L) & G_{(0)}(L, R) \\ G_{(0)}(R, L) & G_{(0)}(R, R) \end{pmatrix} = \\ & 2m \begin{pmatrix} \gamma_L(L, L) + \gamma_B(L, L) & -\gamma_B(L, R) \\ -\gamma_B(R, L) & \gamma_R(R, R) + \gamma_B(R, R) \end{pmatrix}^{-1} = \\ & \frac{2m}{D} \begin{pmatrix} \gamma_R(R, R) + \gamma_B(R, R) & \gamma_B(L, R) \\ \gamma_B(R, L) & \gamma_L(L, L) + \gamma_B(L, L) \end{pmatrix}, \end{aligned} \quad (30)$$

where

$$\begin{aligned} D = & [\gamma_R(R, R) + \gamma_B(R, R)][\gamma_L(L, L) + \gamma_B(L, L)] \\ & - \gamma_B(L, R)\gamma_B(R, L) \end{aligned} \quad (31)$$

and

$$\gamma_\eta(a, b) = -\frac{1}{2m} \partial_x \partial_{x'} g_\eta(x, x'; \omega) \Big|_{x'=b}^{x=a}. \quad (32)$$

The above Green's function is readily cast into a retarded or advanced version by analytically continuing $\omega \rightarrow \lim_{\delta \rightarrow 0^+} \omega \pm i\delta$.

The calculation of $G_{(0)}^<$, however, is significantly complicated through the matrix property (17) inherent to all its defining equations in terms of continuity conditions. The appropriate

choice for these continuity conditions are similar to the ones for $G_{(0)}^{r/a}$ with the only important difference that all first derivatives are continuous also now at $x = x'$. For a general situation with two partitions we find that

$$\begin{aligned}
& \begin{pmatrix} G_{(0)}^<(L, L) & G_{(0)}^<(L, R) \\ G_{(0)}^<(R, L) & G_{(0)}^<(R, R) \end{pmatrix} = -\frac{2m}{|D|^2} \\
& \times \begin{pmatrix} \gamma_R^r(R, R) + \gamma_B^r(R, R) & \gamma_B^r(L, R) \\ \gamma_B^r(R, L) & \gamma_L^r(L, L) + \gamma_B^r(L, L) \end{pmatrix} \\
& \times \begin{pmatrix} \gamma_L^<(L, L) + \gamma_B^<(L, L) & -\gamma_B^<(L, R) \\ -\gamma_B^<(R, L) & \gamma_R^<(R, R) + \gamma_B^<(R, R) \end{pmatrix} \\
& \times \begin{pmatrix} \gamma_R^a(R, R) + \gamma_B^a(R, R) & \gamma_B^a(L, R) \\ \gamma_B^a(R, L) & \gamma_L^a(L, L) + \gamma_B^a(L, L) \end{pmatrix}, \tag{33}
\end{aligned}$$

where it should be noted that despite the presence of the terms with $\gamma_B^<$ in the matrix in the middle, the full Green's function $G_{(0)}^<$ does not depend on these terms. In a true tunneling situation, where one only considers energies lower than the height of the barrier, this is immediately seen to be true since for those energies no states exist in the barrier region. Another case, however, is the one where there are states inside the barrier region in the energy range considered, such as impurity levels or quasi-bound states in a double-barrier tunneling structure; or when a scattering problem across a non-periodic potential is considered rather than a tunneling situation. For these cases one can show¹⁴ that terms in $G_{(0)}^<$ which contain $\gamma_B^<$, occur in conjunction with terms coming from $|D|^{-2}$ and other terms from the matrix product in (33) such that they fulfill an identity $\Delta\delta(\Delta)\Delta \equiv 0$, where Δ is the denominator of γ_B , which is independent of the spatial arguments of γ_B . Put another way, the contributions of the poles in γ_B which constitute $\gamma_B^<$ are suppressed in $G_{(0)}^<$, since wherever they occur they are given zero weight.

One can understand this cancellation from a physical picture of how the nonequilibrium system is established. While the left and right leads are modeled as semi-infinite grand canonical ensembles with (possibly different) chemical potentials on either side at $t = -\infty$,

the barrier region is finite and not coupled to any exterior reservoir. Once a steady state is established, any quantity of the fully coupled system will depend only on the initial occupations of the semi-infinite leads. In particular, there can be no dependence of $G_{(0)}^<$ on $\gamma_B^<$, since the infinite, fully coupled system cannot remember the initial occupation of the finite barrier region. In the same way it turns out that in terms containing $\gamma_B^{r/a}$ only the real part γ_B contributes to $G_{(0)}^<$, as contributions coming from the imaginary parts cancel for the reasons outlined above. Therefore we can set $\gamma_B^< \equiv 0$ and leave away the superscripts in $\gamma_B^{r/a}$ for further calculations.

For the evaluation of (33), however, we still need to know the appropriate expressions for $\gamma_\eta^<$, $\eta \in \{R, L\}$. Since the left and right decoupled regions are separately in equilibrium, they have well defined electron occupations $n_F^\eta(\omega)$, and therefore we find that $g_\eta^<$ can be expressed as

$$g_\eta^<(x, x'; \omega) = n_F^\eta(\omega) \left[g_\eta^a(x, x'; \omega) - g_\eta^r(x, x'; \omega) \right], \quad (34)$$

which immediately transfers to the $\gamma_\eta^<$ as

$$\gamma_\eta^<(x, x'; \omega) = n_F^\eta(\omega) \left[\gamma_\eta^a(x, x'; \omega) - \gamma_\eta^r(x, x'; \omega) \right]. \quad (35)$$

If the impurities lie deeper within the electrodes on the left and right hand sides of the barrier, the relevant Green's functions $G_{(0)}^{r/a}(x_1, x_2)$ and $G_{(0)}^<(x_1, x_2)$ can be expressed in terms of the full Green's functions between the interfaces, (30) and (33), and the Green's functions of the uncoupled leads,

$$\begin{aligned} G_{(0)}^{r/a}(x_1, x_2) &= -(2m)^{-2} \partial_{x'} g_L^{r/a}(x_1, x') \Big|_{x'=L-} \\ &\times G_{(0)}^{r/a}(L, R) \partial_{x'} g_R^{r/a}(x', x_2) \Big|_{x'=R+}, \end{aligned} \quad (36)$$

$$\begin{aligned} G_{(0)}^<(x_1, x_2) &= -(2m)^{-2} \\ &\times \left\{ \partial_{x'} g_L^<(x_1, x') \Big|_{x'=L-} G_{(0)}^a(L, R) \partial_{x'} g_R^a(x', x_2) \Big|_{x'=R+} \right. \\ &\left. + \partial_{x'} g_L^r(x_1, x') \Big|_{x'=L-} G_{(0)}^<(L, R) \partial_{x'} g_R^a(x', x_2) \Big|_{x'=R+} \right. \end{aligned} \quad (37)$$

$$+ \partial_{x'} g_L^r(x_1, x')|_{x'=L-} G_{(0)}^r(L, R) \partial_{x'} g_R^<(x', x_2)|_{x'=R+} \} \\ (x_1 \leq L, \quad x_2 \geq R).$$

The corresponding expressions for the Green's functions with reversed arguments are obtained in an analogous way.

The RKKY interaction (18) can now be expressed entirely in terms of the unperturbed Green's functions of the separate subsystems in equilibrium using (30) and (33)-(37). For the simple case where the impurities are situated immediately on the left and right barrier-electrode interfaces (18) can for example be expressed in terms of the quantities γ_η as

$$E_{\text{RK}} = -2(2m)^2 J^2 \mathbf{S}_1 \cdot \mathbf{S}_2 \int \frac{d\omega}{2\pi} |D|^{-2} \text{Re}[D^{-1}] \gamma_B(L, R) \gamma_B(R, L) \\ \times \text{Im} \{ [\gamma_R^r(R, R) + \gamma_B(R, R)] \gamma_L^<(L, L) + \gamma_R^<(R, R) [\gamma_B(L, L) + \gamma_L^a(L, L)] \}. \quad (38)$$

Within the single effective mass approximation for a barrier system as shown in Fig. 1 the functions of the decoupled leads are found to be

$$g_{L(R)}^{r/a}(x, x') = +(-) \frac{2m}{q_{L(R)}^{r/a}} \\ \times \begin{cases} \sin[q_{L(R)}^{r/a}(x - L(R))] e^{\mp(\pm) i q_{L(R)}^{r/a}(x' - L(R))} & x > (<) x' \\ \sin[q_{L(R)}^{r/a}(x' - L(R))] e^{\mp(\pm) i q_{L(R)}^{r/a}(x - L(R))} & x' > (<) x \end{cases}, \quad (39)$$

where $q_{L(R)}^{r/a} = \sqrt{2m(\omega - V^{L(R)} \pm i\delta)}$, the upper/lower signs are associated with the superscripts r/a, respectively, and $V^{L(R)}$ is the bottom of the conduction band in the corresponding side of the junction as before. Likewise the corresponding Green's functions for the sloping barrier region are obtained as

$$g_B(x, x') = \frac{2m\pi\kappa^{-1}}{f(R)h(L) - f(L)h(R)} \\ \times \begin{cases} [h(L)f(x) - h(x)f(L)] [f(R)h(x') - f(x')h(R)] & x < x' \\ [h(R)f(x) - h(x)f(R)] [f(L)h(x') - f(x')h(L)] & x > x' \end{cases}, \quad (40)$$

where

$$f(x) = \text{Ai}(\kappa x + \zeta/\eta^2), \quad (41)$$

$$h(x) = \text{Bi}(\kappa x + \zeta/\eta^2),$$

are two independent solutions of the inhomogeneous Schrödinger equation

$$\left[\partial_x^2 - \kappa^3 x \right] f(x) = \zeta, \quad (42)$$

with the parameters $\kappa = -\sqrt[3]{\frac{2meV}{R-L}}$ and $\zeta = 2m\{V_0 - eV/2 - \omega\}$.

In equilibrium, where there is no slope to the barrier, one can show that $g_B(x, x')$ simplifies to

$$g_B(x, x') = 2m \begin{cases} \frac{\sinh[k(x-L)] \sinh[k(x'-R)]}{k \sinh[k(R-L)]} & x < x' \\ \frac{\sinh[k(x'-L)] \sinh[k(x-R)]}{k \sinh[k(R-L)]} & x' > x \end{cases}, \quad (43)$$

where $k = \sqrt{2m[V_0 - \omega]}$. Note that (40) and (43) hold for all ω , i.e. including the case when $V_0 - \omega < 0$, for which the sinh-functions in (43) go over to corresponding sin-functions.

When the results of the present and the previous section are combined in equilibrium and for the limit of the barrier height or the barrier width going to zero we can obtain analytic results for all versions of the interaction considered so far. The purely 1D result from (18) for this case reduces to the well known expression for the RKKY interaction in one dimension^{23,24}

$$E_{\text{RK}} = \frac{2m}{2\pi} J^2 \mathbf{S}_1 \cdot \mathbf{S}_2 \left[\text{Si}(\chi) - \frac{\pi}{2} \right], \quad (44)$$

where $\text{Si}(\chi)$ is the integral-sine function

$$\text{Si}(\chi) = \int_0^\chi \frac{\sin(\chi)}{\chi} d\chi \quad (45)$$

and $\chi \equiv 2k_F x$ (with $x \equiv |x_2 - x_1|$) gives the phase of the characteristic oscillation of the interaction at twice the Fermi wavevector k_F .

B. Green's functions in higher dimensions

Once we have found the solutions for the purely 1D Green's functions g_η , which satisfy (26), we can find the solution of the planar extension of the equivalent problem, as demonstrated by (20), by means of Fourier transforms in the directions parallel to the barrier

$$[(\omega - k_\parallel^2/2m) - H_\eta(x)]g_\eta(x, x'; \mathbf{k}_\parallel; \omega) = \delta(x - x'). \quad (46)$$

Here again retarded and advanced versions of $g_\eta^{2/3D}(x, x'; \mathbf{k}_\parallel; \omega)$ can be found simply through continuing analytically

$$g_\eta^{r/a}(x, x'; \mathbf{k}_\parallel; \omega) = g_\eta(x, x'; \mathbf{k}_\parallel; \omega \pm i\delta). \quad (47)$$

Correspondingly we find

$$g_\eta^<(x, x'; \mathbf{k}_\parallel; \omega) = n_F^\eta(\omega) [g_\eta^a(x, x'; \mathbf{k}_\parallel; \omega) - g_\eta^r(x, x'; \mathbf{k}_\parallel; \omega)], \quad \eta \in \{L, R\}. \quad (48)$$

It is important to realize at this point that for the retarded and advanced Green's functions $g_\eta^{r/a}$ the extension to higher dimensions only leads to a shift in the energy argument $\omega \rightarrow \omega - k_\parallel^2/2m$, as can be seen from the form of their defining equation (46), i.e.

$$g_\eta^{r/a}(x, x'; \mathbf{k}_\parallel; \omega) = g_\eta^{r/a}(x, x'; \omega - k_\parallel^2/2m). \quad (49)$$

This property is seen to also translate in part to the functions $g_\eta^<$ with the only important difference that the energy arguments of the occupation functions remain unchanged.

By using the properties (48) and (49) one can establish that the Green's functions of the full system $G_{(0)}^{r/a}$ and $G_{(0)}^<$ can be represented in the following way:

$$G_{(0)}^{r/a}(x, x'; \mathbf{k}_\parallel; \omega) = G_{(0)}^{r/a}(x, x'; \omega - k_\parallel^2/2m), \quad (50)$$

$$G_{(0)}^<(x, x'; \mathbf{k}_\parallel; \omega) = n_F^L(\omega)\Gamma_L(x, x'; \omega - k_\parallel^2/2m) + n_F^R(\omega)\Gamma_R(x, x'; \omega - k_\parallel^2/2m), \quad (51)$$

where the functions Γ_η , $\eta \in \{L, R\}$ associated with the Fermi functions n_F^η can be written in terms of sums and products of spatial derivatives of the $g_\eta^{r/a}$, $\eta \in \{R, B, L\}$ when (30)-(37)

are used to divide $G_{(0)}^<(x, x')$ into contributions containing left or right occupation functions only. For example one finds:

$$\begin{aligned} \Gamma_{L(R)}(L, R) = & -\frac{2m}{|D|^2} \gamma_B(L, R) \left\{ \gamma_{R(L)}^{r(a)}[R(L), R(L)] + \gamma_B[R(L), R(L)] \right\} \\ & \times \left\{ \gamma_{L(R)}^a[L(R), L(R)] - \gamma_{L(R)}^r[L(R), L(R)] \right\}. \end{aligned} \quad (52)$$

The properties (50) and (51) prove to be useful for the evaluation of the frequency and wavevector integrations in the expression for the monolayer interaction (22), which is also needed for the calculation of the slab interaction in (23). If the interaction is considered at zero temperature and the additional property is used that the density of states factor coming from the 2D \mathbf{k}_{\parallel} -integration in (22) is just a constant, one can reduce the three integrations in (22) to a sum of two single integrations as

$$\begin{aligned} & \int \frac{d^2 \mathbf{k}_{\parallel}}{(2\pi)^2} \int_{-\infty}^{\infty} \frac{d\omega}{2\pi} \left[\Theta(\mu - \omega) \tilde{\Gamma}_L(\omega - \frac{k_{\parallel}^2}{2m}) + \Theta(\mu - \omega - eV) \tilde{\Gamma}_R(\omega - \frac{k_{\parallel}^2}{2m}) \right] \\ = & \frac{2m}{8\pi^2} \int_0^{\mu} dz (\mu - z) \tilde{\Gamma}_L(z) + \int_{-eV}^{\mu - eV} dz (\mu - z - eV) \tilde{\Gamma}_R(z), \end{aligned} \quad (53)$$

where the Θ -functions derive from the sharp Fermi distributions $n_F^{\eta}(\omega)$ at $T = 0$ and

$$\tilde{\Gamma}_{\eta}(z) = \text{Im} \left\{ \Gamma_{\eta}(x_1, x_2; z) [G^r(x_2, x_1; z) + G^a(x_2, x_1; z)] \right\}. \quad (54)$$

The lower limits at 0 and $-eV$ in (53) follow from the fact that there are no states below the bottoms of the conduction bands in the left and right lead, respectively. As a result of this simplification the interaction energy between monolayers of spins in 3D is not much harder to evaluate than the interaction energy in the purely 1D case.

For a 3D planar junction in equilibrium without a barrier we find from (22) that the interaction density for monolayers is

$$E_{\text{RK}}^{\text{m}} = \frac{2mk_F^2}{2(2\pi)^2} \left(J\rho_{s-d}^{2D} \right)^2 \nu^{2D} \mathbf{S}_1 \cdot \mathbf{S}_2 \left[\text{Si}(\chi) - \frac{\pi}{2} + \frac{\chi \cos(\chi) - \sin(\chi)}{\chi^2} \right], \quad (55)$$

which is evidently similar to the purely 1D result. The monolayer interaction is therefore often called quasi-one dimensional²³. The slab interaction from (23) in this case assumes the form²⁵

$$E_{\text{RK}}^s = \frac{2m \left(J \rho_{s-d}^{3D} \right)^2 \nu^{2D}}{16(2\pi)^2} \mathbf{S}_1 \cdot \mathbf{S}_2 \{ \mathcal{F}(s+2l) - 2\mathcal{F}(s+l) + \mathcal{F}(s) \}, \quad (56)$$

where $\rho_{s-d}^{3D} = \rho_{s-d}^{1D} \rho_{s-d}^{2D}$ is the 3D density of s - d spins within the slabs, $s = 2d + R - L$ is the spacing between the slabs, l is the width of each slab (see Fig. 2) and $\mathcal{F}(x)$ is the range function

$$\mathcal{F}(x) = \chi^2 \left[\text{Si}(\chi) - \frac{\pi}{2} \right] + \chi \cos(\chi) + \sin(\chi) + 2\text{Si}(\chi), \quad \chi = 2k_F x. \quad (57)$$

Another special case worth noting in this context is the interaction between two magnetic half-spaces separated by a non-magnetic spacer. By letting $l \rightarrow \infty$ we find that (56) simplifies to

$$E_{\text{RK}}^{s\infty} = \frac{2m \left(J \rho_{s-d}^{3D} \right)^2 \nu^{2D}}{16(2\pi)^2} \mathbf{S}_1 \cdot \mathbf{S}_2 \left\{ \left[\chi_s^2 + 2 \right] \left[\text{Si}(\chi_s) - \frac{\pi}{2} \right] + \chi_s \cos(\chi_s) + \sin(\chi_s) \right\}, \quad (58)$$

where $\chi_s = 2k_F s$.

In order to obtain solutions for (18), (22) and (23) also for more general cases we have to perform the corresponding energy integrals numerically.

V. NUMERICAL RESULTS

A. Comparative results in equilibrium

Numerical results for the RKKY interaction across a tunneling junction in equilibrium have been given by Mukasa *et al.*¹⁰ These authors were particularly interested in providing a theoretical model for possible applications in exchange force microscopy, as mentioned in the introduction, which is based on the RKKY interaction as the dominant force between a tunneling tip and a sample. For this purpose Mukasa *et al.* performed an approximate version of scattering wave perturbation theory for free electrons in a 1D system by including the transmission coefficient of an electron tunneling through the barrier at an intermediate stage in their calculation. In contrast, our analytic expression for the RKKY interaction is

exact (to order J^2) since the constituent Green's functions include scattering by the barrier exactly.

In order to compare our results in equilibrium with the ones in Ref. 10, we have implemented our calculation with the same model parameters using a Fermi energy of $\mu \equiv \mu^L = \mu^R = 5.0\text{eV}$ in equilibrium and a lattice constant $a_0 = 2.50\text{\AA}$, along with a Fermi wavevector $k_F = 1.26 \times 10^{10}\text{m}^{-1}$, implying a relative effective electron mass of $m/m_e = 1.20$, where m_e is the bare electron mass. Fig. 3(a) shows plots representing the dimensionless interaction range function $\Phi(x)$ with

$$\Phi(x) = -\pi \left\{ \frac{2m}{2\pi} J^2 \mathbf{S}_1 \cdot \mathbf{S}_2 \right\}^{-1} E_{\text{RK}}(x), \quad (59)$$

where $E_{\text{RK}}(x)$ was obtained from (18) as evaluated in (38). In Fig. 3(a), the impurities are considered to be fixed at the electrode-barrier interfaces, while the width of the barrier is continuously increased from 0.0\AA to 5.0\AA , to represent for example the height of an STM tip above a sample. Without the barrier ($V_0/\mu = 0.0$), the range function reduces to $\Phi(x) = \pi[\pi/2 - \text{Si}(\chi)]$, where $\chi = 2k_F x$.

We have also plotted in Fig. 3(a) the interaction for this case and for a barrier height of $V_0/\mu = 0.5$, where the system is in a scattering state. We find that as the barrier height is increased from zero, the interaction varies with a longer wavelength, corresponding to a decreasing relative wavevector between the top of the barrier and the Fermi level $K_F = \sqrt{2m(\mu - V_0)}$.

For $V_0/\mu > 1$, the strength of the interaction decays exponentially with the width of the barrier, with an exponent that increases with V_0/μ , and the crossover into the antiferromagnetic (AFM) regime is lost once $V_0/\mu \geq 1.3$. In the interval of $V_0/\mu \in [1.0, 1.3]$, the interaction still experiences one slight crossover to the AFM regime. This can be understood to arise from the nature of the transmission and reflection coefficients of the barrier, which are not purely exponential, but a mixture of hyperbolic functions.

However, our results explicitly *do not* show the large oscillation of the interaction far in the ferromagnetic (FM) regime as was obtained in Ref. 10, markedly for their curve

$V_0/\mu = 1.05$. Such a behavior is unphysical in a genuine tunneling situation, and reflects the approximate treatment of the transmission of scattered waves through the barrier in Ref. 10. Our Green's function approach in comparison includes the single particle barrier potential fully from the beginning and therefore allows an exact evaluation of the RKKY interaction.

Other interesting cases to investigate are the interaction of two monolayers, or of two semi-infinite slabs of magnetic impurities in the presence of a tunneling barrier. Such systems could for example be realized by coating both sides of a fixed or mobile tunneling junction with a magnetic material. For these cases one can make use of (22) for monolayers and of (22) and (23) for slabs, both in conjunction with (53). We shall consider (22) in equilibrium and set $eV = 0$ in (53). In Fig. 3(b) and Fig. 3(c) we show results for the interaction range functions

$$\Phi_m(x) = -\pi \left\{ \frac{2mk_F^2}{2(2\pi)^2} (J\rho_{s-d}^{2D})^2 \nu^{2D} \mathbf{S}_1 \cdot \mathbf{S}_2 \right\}^{-1} E_{\text{RK}}^m, \quad (60)$$

$$\Phi_s^\infty(x) = -\frac{\pi}{2} \left\{ \frac{2m (J\rho_{s-d}^{3D})^2 \nu^{2D}}{16(2\pi)^2} \mathbf{S}_1 \cdot \mathbf{S}_2 \right\}^{-1} E_{\text{RK}}^{\infty}, \quad (61)$$

for monolayers and for slabs, respectively, which were obtained for a planar version of the arrangement used for Fig. 3(a). From (55), for zero barrier height, Φ_m reduces to $\Phi_m = \pi\{\pi/2 - \text{Si}(\chi) - [\chi \cos(\chi) - \sin(\chi)]/\chi^2\}$ and Φ_s^∞ to $\Phi_s^\infty = -\pi/2\{[\chi^2 + 2][\text{Si}(\chi) - \pi/2] + \chi \cos(\chi) + \sin(\chi)\}$. The curves in Fig. 3(b) show that characteristically the monolayer interaction Φ_m decays much faster than the purely 1D interaction Φ , shown in Fig. 3(a), when compared with equal parameter values. Especially for $V_0/\mu \geq 1.0$, Φ_m shows a much stronger decay than Φ . This can be understood as a result of the k_{\parallel} -integration in (22) which effectively averages the interaction of one spin on one side of the junction with all other spins on the opposite side. This average which extends over many oscillatory contributions leads to destructive interference effects which results in the observed damping of Φ_m relative to Φ .

When the RKKY interaction of infinite half-spaces represented by Φ_s^∞ is compared to Φ_m and Φ it is seen that the double spatial integration from (23) increases the relative oscillation

strength of Φ_s^∞ when compared to Φ_m , and at $V_0/\mu = 1.05$ the relative cross-over Φ_s into the AFM regime becomes even stronger than the one for Φ .

B. Nonequilibrium behavior

1. Impurities on the electrode-barrier interfaces

In the following we establish how the results shown in Fig. 3 for the interaction in equilibrium are modified when a finite bias is applied to the junction. Fig. 4(a) and Fig. 4(b) show the 1D interaction between two magnetic impurities placed on opposite electrode-barrier interfaces for various strengths of the bias in conjunction with initial equilibrium ratios $V_0/\mu = 1.05$ in Fig. 4(a) and $V_0/\mu = 1.5$ in Fig. 4(b), and with otherwise the same model parameters as in Fig. 3(a).

As the bias is increased in Fig. 4(a) the interaction starts to exhibit oscillations when the right edge of the barrier potential $V(R) = V_0 - eV$ is pulled below the chemical potential of the left hand side μ^L . This oscillation arises because the wavefunctions of high energy electrons tunneling from the left exit the barrier through its sloping part, and become oscillatory over the distance where they are above the barrier. In this regime we find that the wavevector of the oscillation can be roughly approximated by the wavevector of electrons tunneling from the left Fermi level at the position of the right interface with the barrier, i.e.

$$q_F = \sqrt{2m[\mu - V_0 + eV]}, \quad (62)$$

giving an oscillatory wavelength $\Delta x = 2\pi/q_F$. The wavelength of the interaction becomes smaller, i.e. the value of q_F in (62) increases, as the bias is increased. In Fig. 4(a), one can see that as the bias is turned up, the antiferromagnetic region initially vanishes and then almost reappears at a smaller distance between the impurities.

In Fig. 4(b), for $eV/\mu = 1.50$, a similar behavior to the one in Fig. 4(a), for $eV/\mu = 1.05$, is observed. The main difference to Fig. 4(a) is that for $eV/\mu = 1.50$ and in equilibrium the interaction just decays exponentially with no AFM region, whereas out of equilibrium

such an AFM region is established as the bias is turned up. The fact that the oscillations caused by high bias are not centered around the $\Phi = 0$ line in Fig. 4(a) and Fig. 4(b) can be understood to arise from the asymmetric shape of the sloping barrier. From these figures it is apparent that in an arrangement where the impurities are attached to the electrode-barrier interfaces, such as an STM tip and sample, both coated with magnetic materials, the interaction becomes tunable between FM and AFM by varying the bias alone.

Since, as mentioned before, an interesting application of the present system would be in exchange force microscopy — where the force caused by the exchange interaction on a tunneling tip in an STM is measured — we have plotted in Fig. 4(c) and Fig. 4(d) the spatial derivative $-d\Phi(x)/dx$ of the range function $\Phi(x)$ from Fig. 4(a) and Fig. 4(b), respectively. Both Fig. 4(c) and Fig. 4(d) show explicitly that the onset of oscillations in the interaction for an appropriate bias will lead to a force which is alternating in sign. An estimate of the absolute strength of the exchange force and predictions that it should be measurable with a state of the art STM are postponed to a discussion in Sec. VI.

We next consider the effect of a finite bias on a system of two magnetic monolayers interacting across a 3D planar barrier. In Fig. 4(e) and Fig. 4(f) we plot the range function Φ_m , using (22), (53), and (60), for a planar version of the arrangement used in Fig. 4(a) and Fig. 4(b). As in Fig. 4(a) and Fig. 4(b) the interaction starts to exhibit an oscillatory behavior once the slope of the barrier gets steep enough. In both Fig. 4(e) and Fig. 4(f) it is evident that the oscillations can reach into the AFM region, although, as in Fig. 4(a) and Fig. 4(b), the oscillations are again not centered about the $\Phi_m = 0$ line, but are shifted into the FM region.

One more remark is in order when nonequilibrium results for monolayers are compared to results in equilibrium. In equilibrium the total interaction energy E_{RK}^m in (22) is proportional to μ , and we have normalized the range function Φ_m in Fig. 4(e) and Fig. 4(f) with respect to the equilibrium Fermi energy μ . However, the total nonequilibrium interaction from (22) depends in magnitude on a non-separable mixture of μ , eV , $\mu + eV$ and $\mu - eV$. This would be evident if we had plotted the interaction back to $x = 0$ where the results for various

strengths of eV would no longer converge in a single point, as they do in equilibrium for different V_0/μ .

Altogether, our results in Fig. 4(a) and Fig. 4(b) as well as in Fig. 4(e) and Fig. 4(f) show that when the impurities are attached to the electrode-barrier interfaces a switching of the interaction can be achieved in many situations by changing the bias alone, but in general this switching behavior depends quite strongly on the particular properties of the barrier. In the following we will show that such a switching is much more reliably achieved by placing the single spins or layers of spins within the electrodes a finite distance away from the interfaces with the barrier.

2. Impurities within the electrodes

We now consider the nonequilibrium behavior of the interaction when the impurities are placed inside the electrodes a distance d away from the electrode-barrier interfaces. In Fig. 5(a) we show a surface plot of a 1D arrangement with the relative barrier height $V_0/\mu = 1.5$, where the barrier width is kept constant at 1.0\AA [cf. corresponding point in Fig. 4(b)]. The impurities are now moved away from their initial positions on the electrode-barrier interfaces to a maximum distance of $d = 5.0\text{\AA}$ from either interface (plotted across the figure). At the same time the bias is increased from $eV/\mu = 0.0$ to $eV/\mu = 1.5$ (plotted into the depth). We have overlayed a contour plot to make it easier to identify which regions of the surface lie in the FM or AFM regime. The solid zero contour line indicates the boundaries of these regions. In the same way, we show in Fig. 5(b) the interaction density between two monolayers and in Fig. 5(c) the interaction density between two slabs of finite thickness which are placed a finite distance inside two 3D electrodes. The range function in Fig. 5(b) is again normalized with respect to the equilibrium Fermi energy μ . The case of interacting slabs turns out to have quite special features which will be discussed later in this section.

One can see that in both Fig. 5(a) and Fig. 5(b) the interaction is already oscillatory in equilibrium as d is varied, even though $V_0/\mu \geq 1.0$, since now the electrons have to travel over

a finite region on either side of the junction where their wavefunctions are oscillatory. The presence of the barrier in this case leads to an overall exponential damping which reduces the strength of the oscillations everywhere. As the bias is turned up these oscillations evolve into an interference between up to five contributing components which can be explained as follows: To the order of perturbation theory considered, the spins on the left side of the junction interact with the ones on the right through electrons tunneling between the locations of the spins. Electrons in the vicinity of the left spins which are able to perform this process are available up to the Fermi level on the left. The wavevector k_{LL} of the spin polarization of the conduction electrons in the left lead is determined by the cut-offs of the frequency integration in (18) and (22) at the Fermi energy and at the band bottom on the left side V^L , so that $k_{LL} = \sqrt{2m(\mu^L - V^L)}$. This wavevector is, however, a different one, namely $k_{LR} = \sqrt{2m(\mu^L - V^R)}$ once the tunneling electrons have penetrated the barrier and interact with the spin on the right side. The same process applies to the spins on the left feeling the presence of the ones on the right. The corresponding wavevectors involved therefore comprise $k_{ij} = \sqrt{2m(\mu^i - V^j)}$, ($i, j \in \{L, R\}$), i.e. four different ones in principle. In addition to this, one also observes a quite strong oscillation which contains the wavevector $k_{eV} = \sqrt{2meV}$. This oscillation can be understood to arise from the interval in the frequency integration in the expression for the interaction (18) which extends from the band bottom of the right lead to the band bottom of the left lead, i.e. over $V^L - V^R = eV$. Since all cases of the interaction studied here have a one-dimensional or quasi-one-dimensional behavior, both the densities of states of the electrons in the left lead and in the right lead exhibit a singular behavior at the respective band bottoms. The existence of the singular parts of these densities of states at the integration limits gives rise to the $\sqrt{2meV}$ -oscillation, which in some situations becomes the principal oscillation in the nonequilibrium system.

Assuming that μ^R moves by the same amount eV as V^R , and with V^L normalized to zero as shown in Fig. 1, this set of wavevectors reduces to a total of four, namely $k \in \left\{ \sqrt{2m\mu^L}, \sqrt{2m(\mu^L + eV)}, \sqrt{2m(\mu^L - eV)} \right\}$ due to the sharp Fermi distributions n^L and n^R , and the $k_{eV} = \sqrt{2meV}$ oscillation as discussed before. In both Fig. 5(a) and Fig.

5(b), a superposition of these principal wavevectors can be found. Once the bias eV moves the Fermi energy on the right below the band bottom on the left, $\mu^R \leq 0$, the corresponding components of the oscillations turn into an exponential decay, leaving only three contributions to the oscillations. This transition can be seen as a kink in the contour plots in Fig. 5(a) and Fig. 5(b) at a bias of $eV = 1.0$. At higher biases, for arrangements where the impurities lie very close to the barrier, i.e. when $d/(R - L) \ll 1.0$, barrier effects such as those displayed in the plots of Fig. 4(b) and Fig. 4(f) become more important. However, for ratios $d/(R - L) > 1.0$ we expect these effects to be minimal when the width of the barrier is held constant. Both Fig. 5(a) and Fig. 5(b) show explicitly how the interaction between two single spins in 1D and between two layers of spins, respectively, is tunable between ferromagnetic and antiferromagnetic coupling at a fixed impurity configuration by varying the bias alone. Furthermore it is clear in Fig. 5(a) and especially in Fig. 5(b) that the interaction falls off significantly less rapidly in the nonequilibrium regime. This circumstance has particularly strong consequences for the interaction between slabs of spins.

In Fig. 5(c) we have plotted the interaction between two finite magnetic slabs of spins with a width of the slabs of $l = 10\text{\AA}$ using otherwise the same conditions as were taken for the monolayer-case shown in Fig. 5(b). While it can be seen in Fig. 3(c) that in equilibrium the interaction for slabs converges to a finite value in the limit when the thickness of the slabs goes to infinity, $l \rightarrow \infty$, this is no longer the case out of equilibrium. Rather the interaction is seen to become roughly proportional to the thickness of the slabs for thicknesses $l \gg \pi/k_F$. This can be attributed to the longer range of the monolayer interaction as mentioned before, which destroys the quite sensitive convergence of the double integral in (23) for $l \rightarrow \infty$.

When the slab interaction (23) is calculated one can exchange the spatial integrations with the frequency and wavevector integrations. This has the advantage that the spatial integration can be performed analytically first. Since the explicit representation of the integrand is quite involved, we have postponed it to Appendix A. From (A10) it can be seen that the integrand contains several terms which are proportional to l . In equilibrium, as shown in (A8), these terms cancel one another, but out of equilibrium, when the frequency

integration for these terms is cut off at different points through different Fermi occupation functions, this cancellation ceases to be complete. Therefore, when the bias is switched on, a residual l -dependence remains, which increases as the bias is increased. The total interaction energy for slabs therefore scales extensively with the width of the slabs. It should be noted that this extensive dependence of the slab interaction energy out of equilibrium is not caused by the offset of the band bottoms in our model. If an equilibrium system is considered in which materials with different band structures form a junction, the slab interaction continues to converge always [cf. (A8)].

For this reason we have compressed the scale of the plot in Fig. 5(c) in the direction of the bias by a factor of $[1 + 40 \times eV/\mu]^{-1}$, so that, as shown, the height of the oscillations stays approximately the same. Moreover, one can see that the $k_F d$ oscillations observed in equilibrium vanish completely at a very small bias and turn into oscillations with phase $(d/2)\sqrt{2meV}$. That this is the case can be seen from the overlaid contour lines, which, particularly in the upper right corner, show a dependence $\propto 1/\sqrt{2meV}$ when taken as a function of eV . Mathematically, the dominance of these oscillations can be understood to arise from the spatial integrations in formula (23). When the spatial integrations are interchanged with the frequency integration in (23), as it is done in (A1) in Appendix A, the space integrations are effectively taken over products of the oscillatory, i.e. trigonometric, wavefunction-like expressions $\eta_{L(R)}^{r/a}$ from (A2) which relate to electrons in the left and right leads [cf. (A4)-(A7)]. This yields an extra factor of $(q_{L(R)}^{r/a})^{-1}$ in $\xi_{L(R)}^{r/a}$ from (A5). A factor of $\xi_{L(R)}^{r/a}$ occurs at least once in every term in the integrand of the subsequent frequency integration in (A10), which enhances the peak in the quasi-1D density of states of the monolayer system occurring on the bottom of the band in the corresponding lead. The frequency integration itself very much acts as a Fourier transform into real space, which gives the peaks the effect of frequency components of the real-space oscillations of the interaction. These peaks are just an energy interval eV apart, which explains the occurrence of the $k_{eV} = \sqrt{2meV}$ wavevector as a difference wavevector between these components. The strength of k_{eV} is then determined by the strength of the peaks, i.e. the amplitude of the

Fourier components.

Since, as is shown in Fig. 5(c), the interaction between magnetic slabs oscillates with almost only the k_{eV} contribution present, it should be controllable in a simple fashion by tuning the bias.

VI. DISCUSSION

In this section, the possibilities for the experimental study of the RKKY interaction in tunneling systems out of equilibrium are discussed. As mentioned in the introduction, one possible way to probe the behavior of the interaction that we predict is to use an STM to measure the exchange force, such as shown in Fig. 4(c) and Fig. 4(d).

In order to estimate the absolute value of the exchange force, we must estimate J in the prefactor of the force function between two magnetic impurities, adsorbed to the STM tip and the sample, respectively. One method to estimate J , which is also used in Ref. 10, is to use the equation for the Kondo temperature T_K

$$T_K = \frac{\mu}{k_B} \exp \left[-\frac{1}{Jg_{s-d}^{1D}(\mu)} \right], \quad (63)$$

where k_B is the Boltzmann constant and $g_{s-d}^{1D}(\mu) = (2\pi)^{-1} \sqrt{2m/\mu}$ is the 1D density of s - d spin states at the equilibrium Fermi energy μ . For measured T_K 's of about $T_K \sim 100K$ one obtains $Jg_{s-d}^{1D}(\mu) \sim 0.2$. From this the function $F(x)$ representing the total measured exchange force is determined as

$$F = \frac{2m}{2\pi^2} J^2 \mathbf{S}_1 \cdot \mathbf{S}_2 \frac{d\Phi(x)}{dx}. \quad (64)$$

From the parameters introduced above, we find

$$F \sim \mathbf{S}_1 \cdot \mathbf{S}_2 \frac{d\Phi(x)}{dx} \times \mathcal{O}(10^{-20} \text{Nm}), \quad (65)$$

which for the range functions plotted in Fig. 4(c) and Fig. 4(d) leads to forces of about $F \sim \mathcal{O}(10^{-11} \text{N})$. As noted in the literature^{10,26} the resolution of current atomic force microscopy

is about 10^{-11}N — 10^{-13}N , which means that the exchange force should be experimentally observable.

For the observation of the RKKY interaction in layered tunneling systems which exhibit giant magnetoresistance phenomena the results shown in Fig. 5 should give an appropriate prediction. Especially for the case of 3D systems the results for the interaction between interacting slabs of impurities shown in Fig. 5(c) would be most applicable. The most surprising result in this situation is that we find that the interaction scales extensively with the thickness of the slabs. In principle the expression for the interaction we study would diverge in the limit of semi-infinite slabs, but of course this would not be observable in real systems, since processes like spin relaxation or the scattering of electrons on non-magnetic impurities would eventually impose a maximum range on the interaction. However, for slabs of reasonable thickness the switching of the bias should produce an observable change in the decay behavior of the interaction, i.e. in a system with fixed spin positions an anomalous increase of the interaction strength should be measurable.

Furthermore, the tunability of the RKKY interaction in a tunneling system out of equilibrium is particularly interesting in view of the fact that the impurity configuration is normally pre-set in a solid system, which means it is usually not possible to directly observe the oscillatory dependence of the interaction on the impurity spacing. With the present arrangements it becomes possible to observe oscillations of the RKKY coupling via the variation of wavevectors on either side of the junction as the bias is varied. If one follows for example the direction of the bias at a given distance of the spins in any of the contour plots shown in Fig. 5, one can almost always observe at least one crossing from FM to AFM coupling or *vice versa*.

Since, out of equilibrium, as indicated before, the interaction depends on several contributing wavevectors, the relative dependence on these could for example be investigated experimentally by using different materials for the connecting leads and by placing the spins asymmetrically around the barrier, e.g. on the electrode-barrier interface on one side of the junction and further within the electrode on the other side. As the arrangements in Fig.

5(b) and Fig. 5(c) describe routinely achievable physical systems, this suggests that the phenomena found theoretically for such systems should also be accessible to experiment.

VII. CONCLUSION

This paper presents for the first time a theoretical treatment of the RKKY interaction in systems out of equilibrium. Except for processes involving ultrashort time dependent excitations, a proper nonequilibrium situation seems only routinely attainable in structured systems which include a potential barrier. The main achievement of this work is that we have obtained a proper field theoretic description of such a system which is much more systematic than conventional scattering wave perturbation approaches to the problem (cf. Ref. 10). Difficulties such as taking proper account of the different occupation functions in different parts of the system are overcome as well as the problem of how to normalize the wavefunctions involved, since the Green's functions used in the present description are always properly normalized. Our treatment is adaptable to the inclusion of further many-body effects in the problem, such as carrier-carrier interactions in the electrodes and the interaction with phonon modes.

One effect of biasing the system out of equilibrium is that the oscillatory exchange interaction in various dimensions exhibits strong interference effects, leading to one or more changes of the type of coupling (between FM and AFM) at a given impurity configuration as the bias is varied. This behavior arises as a result of an interference between several fundamental oscillations due to a mixing of different wavevectors. The possibility of tuning the interaction through changing the bias alone could become an important effect in applications of nonlinear switching devices using layered magnetic structures with a potential barrier. Another important effect is that out of equilibrium the range of the interaction increases, leading to an interaction energy that scales extensively with the system size in the direction perpendicular to the barrier for interacting slabs of spins. A closer study of this phenomenon for the 3D case presented here, as well as for the 1D case of interacting lines

of spins, where the interaction in equilibrium is known to lead to a helical ordering within each line, is being undertaken.

Our results should be applicable to a very broad variety of conceivable structures and the formalism we have presented here is particularly suitable to be adapted to such situations. Extensions to include varying effective masses and other material properties such as band structure and different band filling in the various sub-parts of the system are obvious. A particular example for a possible extension would be to study the interaction in double or multi-barrier systems out of equilibrium. Furthermore, in order to facilitate a direct comparison to experimental results a next step could include the calculation of the RKKY-perturbed spin-polarized tunneling current across systems of this kind. We also hope our work will encourage the experimental study of giant magnetoresistance phenomena out of equilibrium where one can equally expect interesting interference phenomena to occur as a result of the different relative distances of the Fermi surfaces to the bottoms of the conduction bands involved.

VIII. ACKNOWLEDGMENTS

The authors would like to thank Mr. Carsten Heide at Oxford for reading the manuscript and making useful suggestions. One of the authors (NFS) gratefully acknowledges financial support from NEC for a visit to the NEC Research Institute at Princeton during this collaboration.

APPENDIX A: NONEQUILIBRIUM BEHAVIOR OF THE INTERACTION BETWEEN SLABS

In the expression for the RKKY interaction between 3D slabs of spins from (23), we exchange the spatial integrations with the frequency integral, to obtain

$$E_{\text{RK}}^{\text{s}} = \frac{\left(J\rho_{s-d}^{\text{3D}}\right)^2 \nu^{2\text{D}}}{(2m)^4} \mathbf{S}_1 \cdot \mathbf{S}_2 \int_{-\infty}^{\infty} \frac{d\omega}{2\pi} \int \frac{d\mathbf{k}_{\parallel}^2}{(2\pi)^2} \int_{L-(d+l)}^{L-d} dx_1 \int_{R+d}^{R+(d+l)} dx_2 \quad (\text{A1})$$

$$\text{Im} \left\{ \left[\eta_L(x_1) G_{(0)}(L, R) \eta_R(x_2) \right]^{<} \left[\eta_R^r(x_2) G_{(0)}^r(R, L) \eta_L^r(x_1) + \eta_R^a(x_2) G_{(0)}^a(R, L) \eta_L^a(x_1) \right] \right\}.$$

In (A1) we have used (34) and (35) to rewrite the expression $G_{(0)}^{<}(x_1, x_2)$ $\left[G_{(0)}^r(x_2, x_1) + G_{(0)}^a(x_2, x_1) \right]$ in the integrand. In addition, we have introduced

$$\begin{aligned} \eta_{L(R)}^{r/a}(x_{1(2)}) &= \partial_{x_0} g_{L(R)}^{r/a}(x_{1(2)}, x_0) \Big|_{x_0=L(R)} = \partial_{x_0} g_{L(R)}^{r/a}(x_0, x_{1(2)}) \Big|_{x_0=L(R)} \\ &= +(-)2m \exp \left\{ \mp(\pm) i q_{L(R)}^{r/a} [x_{1(2)} - L(R)] \right\}, \end{aligned} \quad (\text{A2})$$

where $g_{L(R)}^{r/a}(x, x')$ is taken from (39). Furthermore, the explicit frequency and wavevector dependence of the integrand in (A1) was omitted for brevity. The expression for $G_{(0)}^{<}(x_1, x_2) \left[G_{(0)}^r(x_2, x_1) + G_{(0)}^a(x_2, x_1) \right]$ in the integrand can now be further grouped as follows:

$$\begin{aligned} G_{(0)}^{<}(x_1, x_2) \left[G_{(0)}^r(x_2, x_1) + G_{(0)}^a(x_2, x_1) \right] &= \\ (2m)^{-4} \left\{ G_{(0)}^{<}(L, R) G_{(0)}^r(R, L) [\eta_L^r(x_1)]^2 \eta_R^r(x_2) \eta_R^a(x_2) \right. \\ &+ G_{(0)}^{<}(L, R) G_{(0)}^a(R, L) \eta_L^r(x_1) \eta_L^a(x_1) [\eta_R^a(x_2)]^2 \\ &+ G_{(0)}^r(L, R) G_{(0)}^r(R, L) [\eta_L^r(x_1)]^2 \eta_R^r(x_2) \eta_R^{<}(x_2) \\ &+ G_{(0)}^a(L, R) G_{(0)}^a(R, L) \eta_L^{<}(x_1) \eta_L^a(x_1) [\eta_R^a(x_2)]^2 \\ &+ G_{(0)}^r(L, R) G_{(0)}^a(R, L) \eta_L^r(x_1) \eta_L^a(x_1) \eta_R^a(x_2) \eta_R^{<}(x_2) \\ &\left. + G_{(0)}^a(L, R) G_{(0)}^r(R, L) \eta_L^{<}(x_1) \eta_L^r(x_1) \eta_R^r(x_2) \eta_R^a(x_2) \right\}. \end{aligned} \quad (\text{A3})$$

When now the functions $\eta^{<}$ are replaced by their definitions in terms of retarded and advanced functions, $\eta_{L(R)}^{<} = n_F^{L(R)} \left[\eta_{L(R)}^a - \eta_{L(R)}^r \right]$, one can see that all occurring dx_1 and dx_2 integrations can be accounted for by introducing the following terms:

$$\begin{aligned} \xi_{L(R)}^0 &= \int_{L-d-l}^{L-d} \left(\int_{R+d}^{R+d+l} \right) dx_{1(2)} \eta_{L(R)}^r(x_{1(2)}) \eta_{L(R)}^a(x_{1(2)}) \\ &= \frac{(2m)^2 i}{q_{L(R)}^a - q_{L(R)}^r} \left\{ \exp \left[i(q_{L(R)}^r - q_{L(R)}^a)(d+l) \right] - \exp \left[i(q_{L(R)}^r - q_{L(R)}^a)d \right] \right\} \\ &= \begin{cases} (2m)^2 l, & \omega - V^{L(R)} \geq 0 \\ -\frac{(2m)^2}{2\sqrt{2m(V^{L(R)} - \omega)}} \left\{ \exp \left[-2\sqrt{2m(V^{L(R)} - \omega)}(d+l) \right] \right. \\ \quad \left. - \exp \left[-2\sqrt{2m(V^{L(R)} - \omega)}d \right] \right\}, & \omega - V^{L(R)} < 0 \end{cases}, \end{aligned} \quad (\text{A4})$$

$$\begin{aligned}\xi_{L(R)}^{r/a} &= \int_{L-d-l}^{L-d} \left(\int_{R+d}^{R+d+l} \right) dx_{1(2)} [\eta_{L(R)}^{r/a}(x_{1(2)})]^2 \\ &= \mp \frac{(2m)^2 i}{2q_{L(R)}^{r/a}} \left\{ \exp \left[\pm 2i q_{L(R)}^{r/a} (d+l) \right] - \exp \left[\pm 2i q_{L(R)}^{r/a} d \right] \right\}.\end{aligned}\quad (\text{A5})$$

While $\xi_{L(R)}^0$ from (A4) produces a term proportional to l for energies above the band bottom in the respective lead, it is seen from (A4) and (A5) that

$$\xi_{L(R)}^0 = \xi_{L(R)}^{r/a}, \quad \omega - V^{L(R)} < 0. \quad (\text{A6})$$

From here we find

$$\begin{aligned}& \int_{L-(d+l)}^{L-d} dx_1 \int_{R+d}^{R+(d+l)} dx_2 G_{(0)}^<(x_1, x_2) \left[G_{(0)}^r(x_2, x_1) + G_{(0)}^a(x_2, x_1) \right] = \\ & (2m)^{-4} \left\{ G_{(0)}^<(L, R) G_{(0)}^r(R, L) \xi_L^r \xi_R^0 + G_{(0)}^<(L, R) G_{(0)}^a(R, L) \xi_R^a \xi_L^0 \right. \\ & + G_{(0)}^r(L, R) G_{(0)}^r(R, L) n_F^R(\omega) \xi_L^r \left[\xi_R^0 - \xi_R^r \right] + G_{(0)}^a(L, R) G_{(0)}^a(R, L) n_F^L(\omega) \xi_R^a \left[\xi_L^a - \xi_L^0 \right] \\ & \left. + G_{(0)}^r(L, R) G_{(0)}^a(R, L) n_F^R(\omega) \xi_L^0 \left[\xi_R^a - \xi_R^0 \right] + G_{(0)}^a(L, R) G_{(0)}^r(R, L) n_F^L(\omega) \xi_R^0 \left[\xi_L^0 - \xi_L^r \right] \right\}.\end{aligned}\quad (\text{A7})$$

Since the problem we consider has time-reversal symmetry, $G_{(0)}^{r/a}(L, R) = G_{(0)}^{r/a}(R, L)$ always holds. When (A7) is considered in equilibrium, we know that also $G_{(0)}^<(L, R) = n_F(\omega) \left[G_{(0)}^a(L, R) - G_{(0)}^r(L, R) \right]$ holds. In such a situation it is seen that (A7) simplifies to

$$\begin{aligned}& \int_{L-(d+l)}^{L-d} dx_1 \int_{R+d}^{R+(d+l)} dx_2 G_{(0)}^<(x_1, x_2) \left[G_{(0)}^r(x_2, x_1) + G_{(0)}^a(x_2, x_1) \right] = \\ & n_F(\omega) \left\{ \left[G_{(0)}^a(L, R) \right]^2 \xi_L^a \xi_R^a - \left[G_{(0)}^r(L, R) \right]^2 \xi_L^r \xi_R^r \right\},\end{aligned}\quad (\text{A8})$$

where it was assumed that ξ_L and ξ_R may also be different in equilibrium, e.g. if the materials on the left and right of the junction have different work functions. Clearly in (A8) all factors proportional to l have vanished as expected. When l is taken to $l \rightarrow \infty$ the functions $\xi_{L(R)}^{r/a}$ oscillate with l , as is seen from (A5), and eventually reduce to

$$\lim_{l \rightarrow \infty} \xi_{L(R)}^{r/a} = \pm \frac{(2m)^2 i}{2q_{L(R)}^{r/a}} \exp \left[\pm 2i q_{L(R)}^{r/a} d \right], \quad (\text{A9})$$

due to the retarded/advanced property of the $q_{L(R)}^{r/a}$, which causes an exponential decay in the relevant functions at large distances.

Out of equilibrium, however, the cancellation of the l -proportionality ceases to be complete and the expression for the slab interaction (23) can be rewritten by means of (52) and (53) for zero temperature as

$$E_{\text{RK}}^s = \frac{\left(J\rho_{s-d}^{3\text{D}}\right)^2 \nu^{2\text{D}}}{8\pi^2(2m)^3} \mathbf{S}_1 \cdot \mathbf{S}_2 \quad (\text{A10})$$

$$\times \left\{ \int_0^\mu dz(\mu - z) \text{Im} \left[\left(\Gamma_L(z) - G_{(0)}^a(z) \right) \Xi(z) + \left(G_{(0)}^a(z) \right)^2 \xi_L^a(z) \xi_R^a(z) \right] \right.$$

$$\left. + \int_{-eV}^{\mu-eV} dz(\mu - z - eV) \text{Im} \left[\left(\Gamma_R(z) + G_{(0)}^r(z) \right) \Xi(z) - \left(G_{(0)}^r(z) \right)^2 \xi_L^r(z) \xi_R^r(z) \right] \right\},$$

where we have introduced

$$\Xi(z) = G_{(0)}^r(z) \xi_L^r(z) \xi_R^0(z) + G_{(0)}^a(z) \xi_R^a(z) \xi_L^0(z), \quad (\text{A11})$$

with the abbreviation: $G_{(0)}(L, R; z) = G_{(0)}(z)$ and $\Gamma_{L(R)}(L, R; z) = \Gamma_{L(R)}(z)$. Note that in (A10) terms containing $\xi_L^0 \xi_R^0 G_{(0)}^r(z) G_{(0)}^a(z)$ have vanished, since they are entirely real. From the definition of the $\xi_{L(R)}^0$ in (A4) it is seen that the term $\Xi(z)$ from (A11) is proportional to l for $z \geq 0$. When $-eV < z < 0$, $\Xi(z)$ always has one l -proportional and one exponentially decaying component, where the latter describes the penetration of low-lying electron states in the right lead to the position of the spins in the left one. The l -proportional component, however, vanishes for energies below zero, since in this case the term $\left[\Gamma_R(z) + G_{(0)}^r(z) \right] G_{(0)}^r(z) \xi_L^r(z) \xi_R^0(z)$ turns out to be entirely real. The remaining l -dependence of $\Xi(z)$ subsequently translates to the slab interaction from (A10) for energies $z \geq 0$, where it is seen to produce terms proportional to l , i.e. which scale extensively with the thickness of the slabs, as well as the equilibrium terms from (A8) before, which show no l -proportionality.

REFERENCES

- ¹ M.A. Ruderman, C. Kittel, *Phys. Rev.* **96**, 99 (1954).
- ² K. Yosida, *Phys. Rev.* **106**, 893 (1957).
- ³ T. Kasuya, *Prog. Theor. Phys.* **16**, 45 (1956).
- ⁴ M.D. Stiles, *Phys. Rev.* **B 48**, 7238 (1993).
- ⁵ P. Grünberg, R. Schreiber, Y. Pang, M.B. Brodsky, H. Sowers, *Phys. Rev. Lett.* **57**, 2442 (1986).
- ⁶ M.N. Baibich, J.M. Boto, A. Fert, F. Nguyen Van Dau, F. Petroff, P. Etienne, G. Creuzet, A. Friederich, J. Chazelas, *Phys. Rev. Lett.* **61**, 2472 (1988).
- ⁷ S.S.P. Parkin, N. More, K.P. Roche, *Phys. Rev. Lett.* **64**, 2304 (1990).
- ⁸ R. Meservey, P.M. Tedrow, *Phys. Rep.* **238**, 173 (1994).
- ⁹ D.T. Pierce, *Phys. Scr.* **38**, 291 (1988).
- ¹⁰ K. Mukasa, H. Hasegawa, Y. Tazuke, K. Sueoka, M. Sasaki, K. Hayakawa, *Jpn. J. Appl. Phys.* **33**, 2692 (1993).
- ¹¹ L.V. Keldysh, *Soviet Physics JETP* **20**, 1018 (1965).
- ¹² C. Caroli, R. Combescot, P. Nozières and D. Saint-James, *J. Phys.* **C 4**, 916 (1971).
- ¹³ C. Caroli, R. Combescot, P. Nozières, D. Lederer and D. Saint-James, *J. Phys.* **C 4**, 2598 (1971).
- ¹⁴ R. Combescot, *J. Phys.* **C 4**, 2611 (1971).
- ¹⁵ C. Caroli, R. Combescot, P. Nozières and D. Saint-James, *J. Phys.* **C 5**, 21 (1972).
- ¹⁶ T.E. Feuchtwang, *Phys. Rev.* **B 10**, 4121 (1974).
- ¹⁷ T.E. Feuchtwang, *Phys. Rev.* **B 10**, 4135 (1974).

- ¹⁸ T.E. Feuchtwang, *Phys. Rev. B* **13**, 517 (1976).
- ¹⁹ C. Kittel, *Quantum Theory of Solids*, 360, Wiley, New York (1987).
- ²⁰ G.D. Mahan, *Many Particle Physics* (Plenum, New York, 1990), pp. 17 – 125.
- ²¹ R.H. Bresemann, M. Bailyn, *Phys. Rev.* **154**, 471 (1967).
- ²² J.A. Blackman, R.J. Elliott, *J. Phys.* **C 2**, 1670 (1970).
- ²³ Y. Yafet, *Phys. Rev. B* **36**, 3948 (1987).
- ²⁴ U. Larsen, *Physics Letters* **85 A**, 471 (1981).
- ²⁵ W. Baltensperger, J.S. Helman, *Appl. Phys. Lett.* **57**, 2954 (1990).
- ²⁶ Y. Martin, C.C. Williams, H.K. Wickramasinghe, *J. Appl. Phys.* **61**, 4723 (1987).

FIGURES

FIG. 1. Schematic representation of the one dimensional tunneling system described in the text. Two magnetic s - d impurities are situated in the left and right lead at equal distances d away from the electrode-barrier interfaces L and R , respectively, and interact with each other through the tunneling of electrons across the barrier. The points L and R at the same time serve as the partitioning points within the Caroli/Feuchtwang formalism, indicated by the two dashed vertical lines.

FIG. 2. Cross-sectional drawing of a magnetic multilayer structure, obtained as a 3D planar extension of the 1D system shown in Fig. 1. Two magnetic slabs M are separated by non-magnetic spacer layers S and a planar tunneling barrier B extending between points L and R . The spins in the magnetic slabs are assumed to have the same orientation within each slab due to a dominance of ferromagnetic (FM) coupling at short distances.

FIG. 3. Range functions: (a) $\Phi(x)$ for interacting magnetic impurities in 1D from (59), (b) $\Phi_m(x)$ for interacting magnetic monolayers in 3D from (60), and (c) $\Phi_s^\infty(x)$ for semi-infinite interacting magnetic slabs in 3D from (61) plotted against the distance $x = R - L$ between the spins in equilibrium, where the spins are considered to be fixed on either interface of the barrier ($d = 0$). The barrier width is increased from 0.0\AA to 5.0\AA and the height of the barrier is increased throughout the plots as indicated. For $V_0/\mu = 0.0$ (a), (b) and (c) show the range functions $\Phi(x)$, $\Phi_m(x)$ $\Phi_s^\infty(x)$, respectively, for a free electron system.

FIG. 4. (a),(b): range function $\Phi(x)$ from (59), (c),(d): force function $-d\Phi(x)/dx$, and (e),(f): range function $\Phi_m(x)$ from (60) for finite bias eV . The initial relative barrier height in equilibrium is fixed at (a),(c),(e): $V_0/\mu = 1.05$ and (b),(d),(f): $V_0/\mu = 1.50$ with otherwise the same system parameters as in Fig. 3 (μ is the Fermi energy of the leads in equilibrium). In four steps a bias eV of up to $eV/\mu = 2.0$ is applied to the junction.

FIG. 5. Surface plot of the range function (a): Φ , (b): Φ_m and (c): $\Phi'_s = [1 + 40 \times eV/\mu]^{-1} \Phi_s^{l=10}$ when the impurities are moved within the electrodes. In the present arrangement the barrier height is fixed to $V_0/\mu = 1.50$ and the barrier width to $R - L = 1.0\text{\AA}$. The distance d of the impurities on either side of the barrier is increased from $d = (0.0 - 5.0)\text{\AA}$ (plotted across), while at the same time the bias is varied from $eV = (0.0 - 1.5)\text{eV}$ (plotted into depth). The thickness of the slabs in (c) was taken to be $l = 10\text{\AA}$. In (a), (b) and (c) the front faces of the surfaces show the equilibrium range functions, which are oscillatory as the spins are moved through the leads. In order to be able to better identify the boundaries between FM and AFM regions, we have overlayed a contour plot showing the zero coupling ($\Phi = 0$) contour.

Figure 4

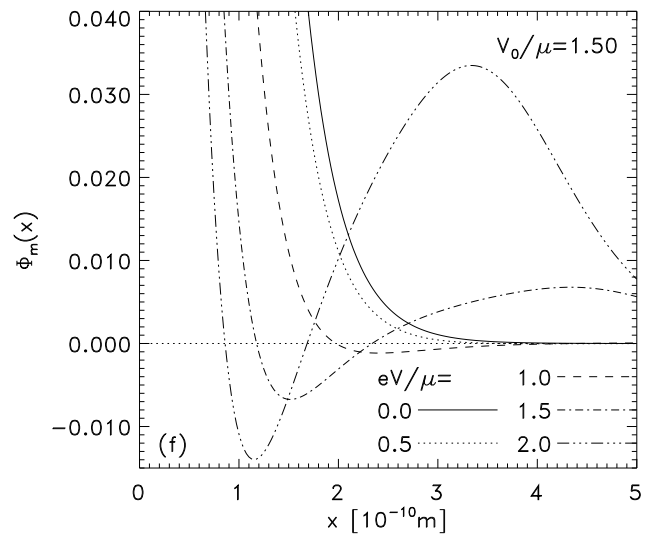
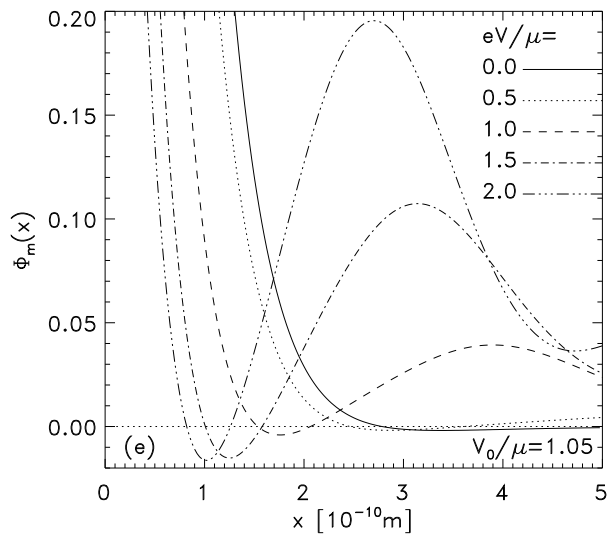
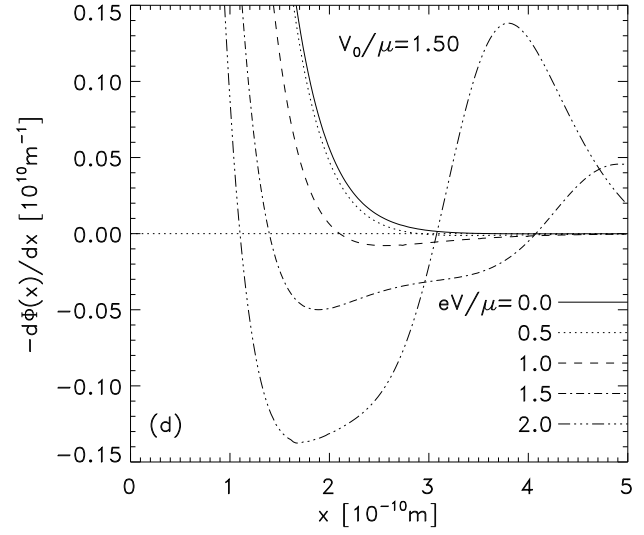
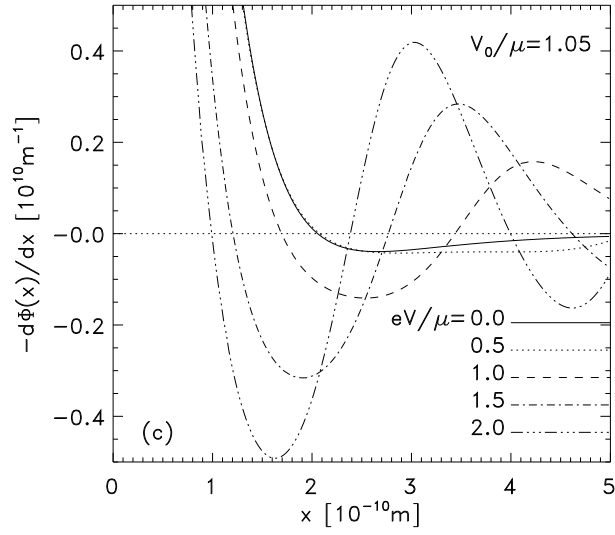
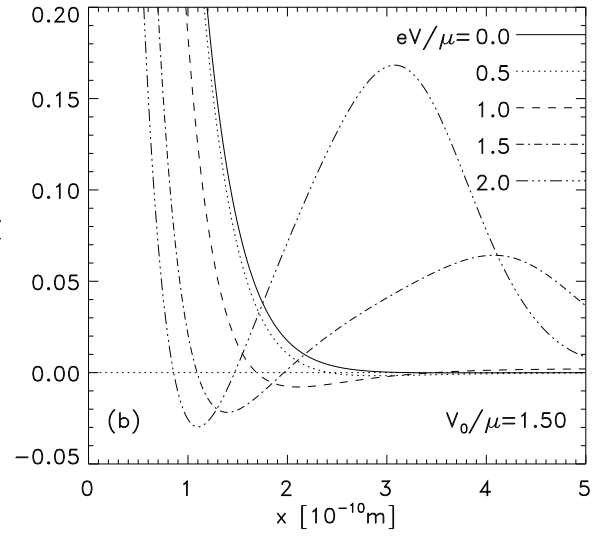
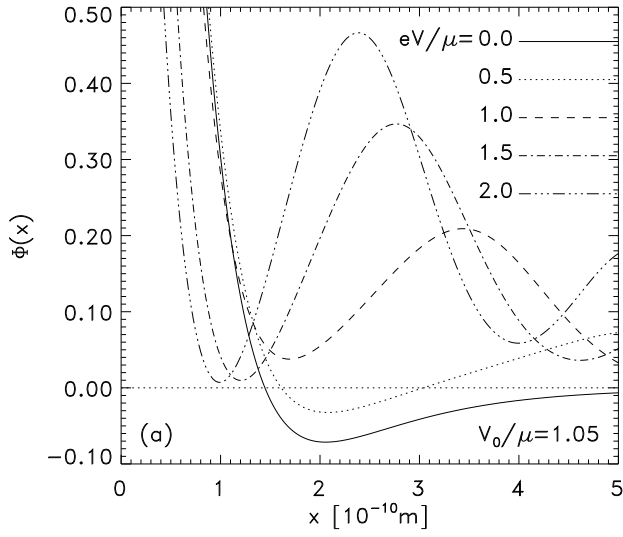


Figure 1

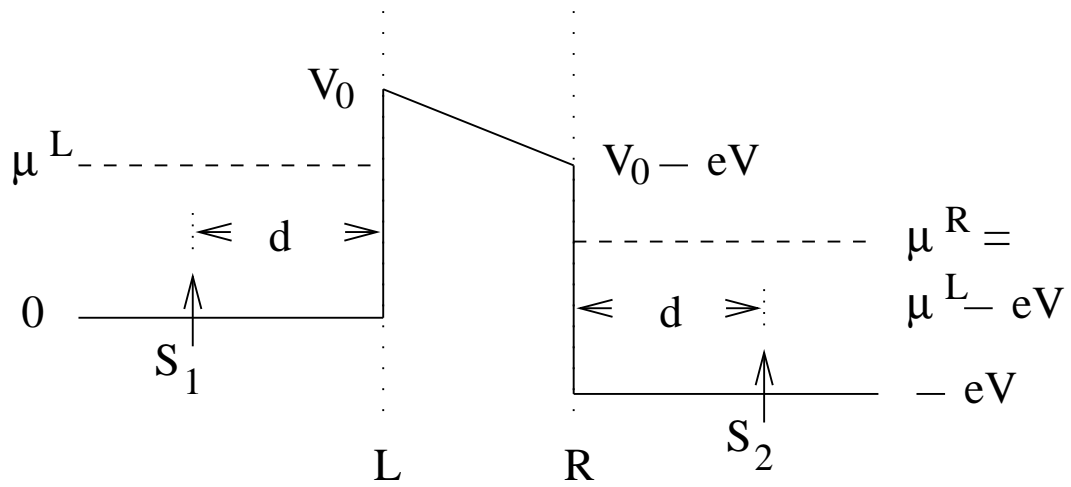


Figure 2

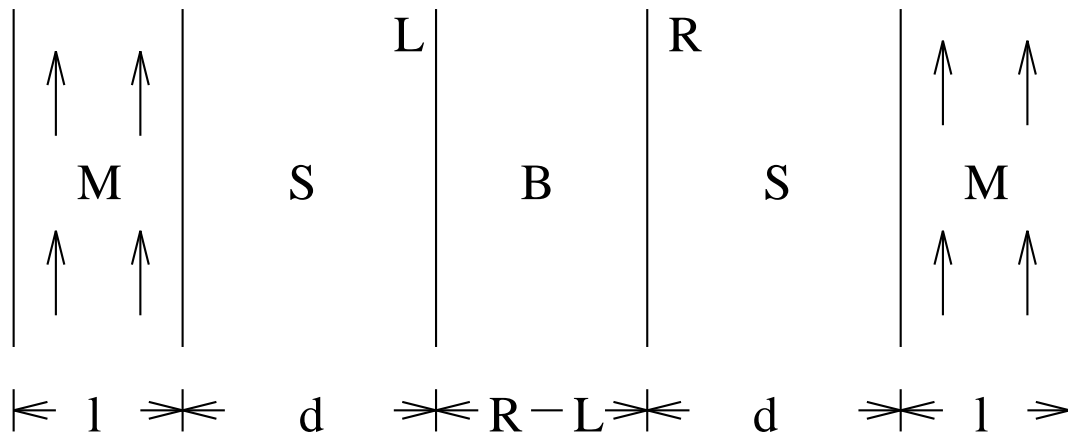


Figure 3

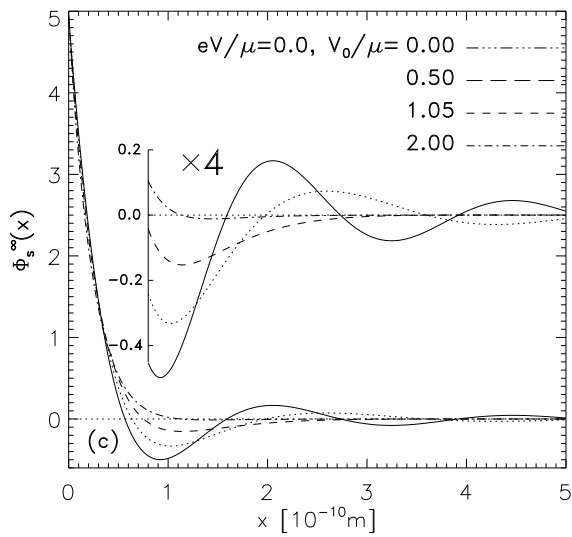
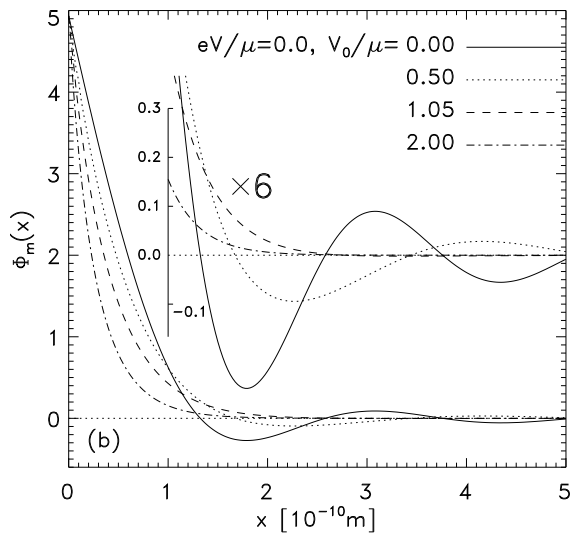
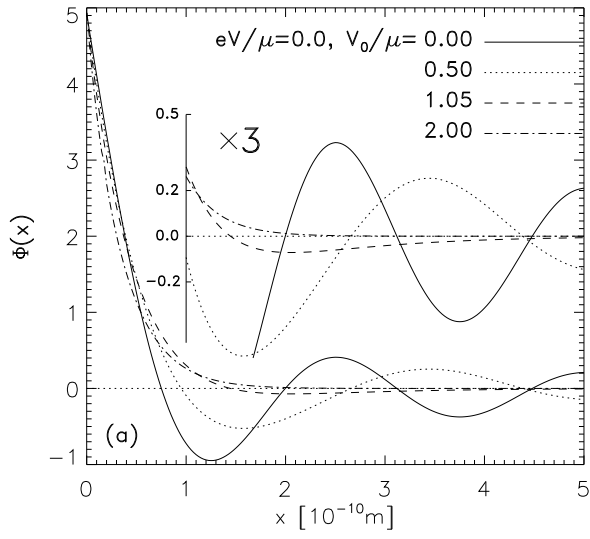


Figure 5

